

Full Length Article

Dynamic characterization of residual oil during long-term waterflooding experiments in heterogeneous porous structures

Wenbo Gong^a, Yang Liu^a, Chaodong Xi^a, Guang Yang^a, Yang Ju^b, Moran Wang^{a,*}

^a Department of Engineering Mechanics, Tsinghua University, Beijing 100084, China

^b State Key Laboratory of Coal Resources & Safe Mining, China University of Mining & Technology, Beijing 100083, China

ARTICLE INFO

Keywords:

Residual oil classification
Pore-scale displacement mechanism
Dynamic characterization
Long-term waterflooding
Heterogeneous porous structures

ABSTRACT

To improve the understanding of trapping and mobilization mechanism during multiphase flow in porous media, long-term waterflooding experiments have been performed to capture the water–oil displacement behaviors in sandstone cores with different permeability and porosity. The residual oil is therefore categorized based on force analysis and morphological characteristics. The critical values for categorization are determined by measuring differences using statistical evaluation. Simplified models of five types of residual oil are established and the dynamic variations of types and volumes of residual oil are characterized during the long-term waterflooding in the sandstone cores. The results indicate that the pore structure heterogeneity impacts the force balance and morphology of residual oil, leading to various dominant types in the sandstone cores with different permeability. Moreover, for effective mobilization of the residual oil, different strategies of enhanced oil recovery are designed controlling the force balance of residual oil. The strategies for oil mobilization are validated by the dynamic pore network modeling, and the enhanced oil recovery is up to 28 %. This study provides a new classification method of residual oil and corresponding mobilization strategies from the perspective of force balance and morphology, which is vital to enhance oil recovery in the high/ultra-high water-cut stage of the oil reservoirs.

1. Introduction

How to accurately characterize and ultimately recover more residual oil is a significant issue not only in conventional mature oilfields but also in other unconventional and deep-buried oilfields [1]. The long-term waterflooding brought about preferential flow paths in the reservoir rocks, leading to serious channeling phenomena and crossflow in the subsurface. This affects the spread of injecting water, increasing the reservoir water production and decreasing the ultimate oil recovery, leading to a high water content exceeding 90 % in crude oil production [2]. About 25 %–50 % of the oil is left unrecovered in the sweeping zone during the waterflooding process, which is the residual oil saturation, also called the trapped oil saturation [3].

Previous studies have demonstrated a wide disordered distribution of trapped phase in the sweeping zone of heterogeneous porous structure [4–8]. The trapped oil is the main object of enhanced oil recovery in high water-cut oilfields [9,10]. One of the challenges is to figure out the pore-scale distribution and saturation changes of the trapped oil in the reservoir rocks [11,12]. Currently, the physical experimental technique is the main approach to investigate the distribution and re-enrichment

transport of trapped oil at the pore scale [13], including the microscopic-physical model [14] and the small-core model [15]. Microscopic-physical model refers to completing waterflooding experiments based on a micro-model generated by light-chemical etching, the thin section of rock core, or the three-dimensional (3D) printing technique, combined with imaging techniques such as optical microscopy, to intuitively show the distribution of residual oil within pore structures [16–18]. The small-core experiment is conducted using high-resolution CT imaging equipment [19], which could visualize the morphology of the solid-water–oil phases in a 3D digital model by reconstructing the CT images [8,20–23]. Using the CT scanning technique, scholars discussed the factors on the occurrence state and trapping of residual oil, including the pore structure heterogeneity [21], reservoir permeability difference [24], rock mineral components [25], and fluid wettability distribution [7,26,27]. To distinguish the residual oil types, various parameters are used to characterize the residual oil distribution, such as shape factor, contact area ratio, Euler characteristic number, interface curvature, occupied pore number, and pore-throat number, forming versatile oil classification that includes film-like, droplet-like, porous, columnar, and continuous cluster-like residual oil [28–30]. There is still a lack of

* Corresponding author.

E-mail address: mrwang@tsinghua.edu.cn (M. Wang).

<https://doi.org/10.1016/j.fuel.2023.129567>

Received 27 May 2023; Received in revised form 4 August 2023; Accepted 19 August 2023

Available online 27 August 2023

0016-2361/© 2023 Elsevier Ltd. All rights reserved.

understanding about how to choose the reasonable parameters to identify the occurrence state of residual oil and then to stimulate an effective recovery strategy.

Previous research on residual oil focuses on the qualitative understanding of macroscopic property changes, lacking effective quantitative characterization and corresponding insights at the pore scale, which cannot meet the needs of the efficient exploitation of highly dispersed and diversified residual oil. The residual oil is described almost based on the morphological characteristics [31–34], and the numerical simulation is used to analyze their remobilization conditions in heterogeneous porous structure [35,36]. It is practicable to identify the residual oil by the morphological characteristics, while it is challenging to serve the understanding of the fluid dynamic behaviors including trapping and mobilization of residual oil. Owing to the high heterogeneity of pore structure in reservoir rocks, the interior residual oil after waterflooding is distributed within the small pores in the form of an overall scattered and locally enriched pattern. The heterogeneity of local structure and wettability in the rocks lead to various force types acting on the residual oil [37–39], and the force difference at the pore scale determines its occurrence state and subsequent mobilization conditions. The residual oil trapped in the pores is controlled by the combined effect of displacement pressure, gravity, buoyancy, capillary force, and viscous force [40–43]. During long-term waterflooding, the force balance state of the trapped phase in porous media is usually destroyed due to the long-term flushing shearing effect and pressure disturbance. When the driving force is greater than the resistance, the trapped oil will be remobilized. The rocks collected from different oil reservoirs have significantly different characteristics in terms of porosity, pore size distribution, and permeability [44,45], which causes uncertainty about the dominant driving forces and the variation of the residual oil distribution. Therefore, it is necessary to propose a general method to identify the controlling factor in the dynamic variations of residual oil during long-term waterflooding from the perspective of force analysis and fluid mechanics in porous media. Besides, a few quantitative parameters are used in the classification of residual oil, while it is difficult to relate these morphological parameters to the multiphase flow, and there is no specific approach to determine the critical value of these parameters for the residual oil in porous media. To study residual oil in high water-cut oilfields, it is urgently needed to establish the dynamic characterization methods for residual oil variation in the heterogeneous porous structures and analyze the pore-scale forces acting on the residual oil to further clarify its residual state and effective mobilization.

To characterize the dynamics of the residual oil in the heterogeneous porous structures, the long-term waterflooding experiments were performed in sandstone rocks with various permeability, and the interior oil–water distribution at different waterflooding stages was captured using micro-CT scanning technique. Moreover, this study proposes a novel analysis method considering the force balance and morphological characteristics of residual oil, including the residual oil classification, determination of critical values for categorized parameters, and identifying oil mobilization conditions. The corresponding strategies of oil mobilization are validated using the pore-scale simulation. Our findings can offer valuable insight into the effect of pore structure characteristics on the oil trapping in porous media, and an understanding of the distribution patterns and effective remobilization of residual oil. This will assist in accurately evaluating the occurrence state of residual oil and formulating strategies for residual oil exploitation in high water-cut reservoirs.

2. Materials and methods

2.1. The sandstone rock samples

To investigate the distribution and variation of residual oil at the pore scale, natural cores in the sandstone reservoir with different permeability were used for long-term waterflooding experiments in this

study. The sandstone samples are selected from the different layers of the Lamadian Formation of Daqing oilfields in China, which is located in the continental river-delta sandstone reservoir with medium and high permeability. The rock sample (Rock 1) is classified as fine sandstone, and other rocks (i.e., Rock 2 and Rock 3) are silty sandstone, according to the particle size of sandstone rocks. The main mineral components of the sandstone samples are quartz and feldspar minerals, which together account for more than 90 %. The clay content is about 3–7 %. The porosity and permeability of samples measured experimentally are 29.64 % and 7449 mD in Rock 1, 31.09 % and 1594 mD in Rock 2, and 29.22 % and 908 mD in Rock 3 (see Table 1).

Three-dimensional (3D) reconstruction technology based on CT scanning was used to extract the pore structure information from the natural cores. The reconstructed digital rocks of pore structure went through digital analysis including 3D visualization and pore size distribution, as shown in Fig. 1. It is noteworthy that the voxel resolution of CT scanning is 1.91 $\mu\text{m}/\text{voxel}$ edge for the measured samples. A wider pore size distribution is related to the sandstone core with higher permeability, and the average pore diameters of the interior pore structure in Rock 1, Rock 2, and Rock 3 are 71.4, 47.8, and 39.6 μm , respectively.

2.2. Long-term waterflooding experiments

The rock and fluids were imaged using an Xradia MicroXCT-400 X-ray Microscope. A high-resolution microscopy detector is used with a pixel of 2048×2048 and a resolution of 1.91 μm . The view field along the vertical direction contains 2000 image slices. During the CT scanning, the voltage and power of the equipment are set at 150 kV and 10 W. The exposure time is set as 0.5 s. Fig. 2 shows the experiment process of long-term waterflooding in natural cores. To enhance the gray value contrast and allow phase segmentation in CT images, the brine fluid containing 10 wt % sodium iodide is used as the water phase, and the liquid paraffin is selected as the oil phase in the two-phase displacement experiments, owing to their contrast in terms of the relative X-ray intensity. The fluid density and viscosity are 1.12 g/cm^3 and 1.2 mPa·s, 0.84 g/cm^3 and 7.5 mPa·s for water and oil phase, respectively. The oil–brine interfacial tension is 30 mN/m. The wettability of sandstone samples is represented by the average contact angle measured from the three-phase contact line in the rock sample saturated with oil and brine [46], and the calculated contact angles are 83.1°, 80.8°, and 76.8° for Rock 1, Rock, and Rock 3, respectively. The wettability condition is the weakly hydrophilic state. During the experimental preparation stage, the dried sandstone core was vacuumed and saturated with brine, pressurized to 20 MPa to age 7 days, and then the sample is put into the core chamber connecting to the experimental system of immiscible displacement. To simulate the coexistence of water–oil in the rock, the oil phase is injected into the rock sample saturated with brine with a pump flow rate of 8.3 $\mu\text{L}/\text{min}$, temperature of 25 °C, and confining pressure of 5 MPa until no water production in the outlet. After the experimental system stands for 12 h to reach the dynamic equilibrium between the rock matrix and pore fluid, the state of water–oil distribution in the rock sample is recorded as the initial stage, OPV. Finally, the long-term waterflooding experiment is conducted in the rock sample with brine injection, as shown in Fig. 2. We extracted the information of pore structure and water–oil distribution at seven displacement stages during the waterflooding experiment using CT scanning test. The selected displacement stages are OPV, 0.5PV, 1PV, 3PV, 10PV, 50PV,

Table 1
The pore structure characteristics in different sandstone rocks.

Samples	Porosity	Permeability	Mean Size
Rock 1	29.64 %	7449 mD	71.4 μm
Rock 2	31.09 %	1594 mD	47.8 μm
Rock 3	29.22 %	908 mD	39.6 μm

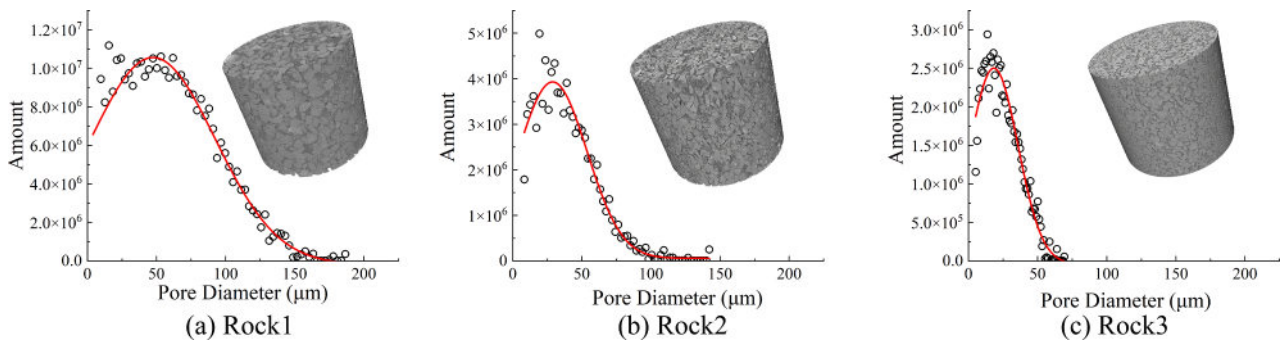


Fig. 1. The pore size distribution of various sandstone cores from the digital rock analysis: (a) Rock 1, (b) Rock 2, and (c) Rock 3.

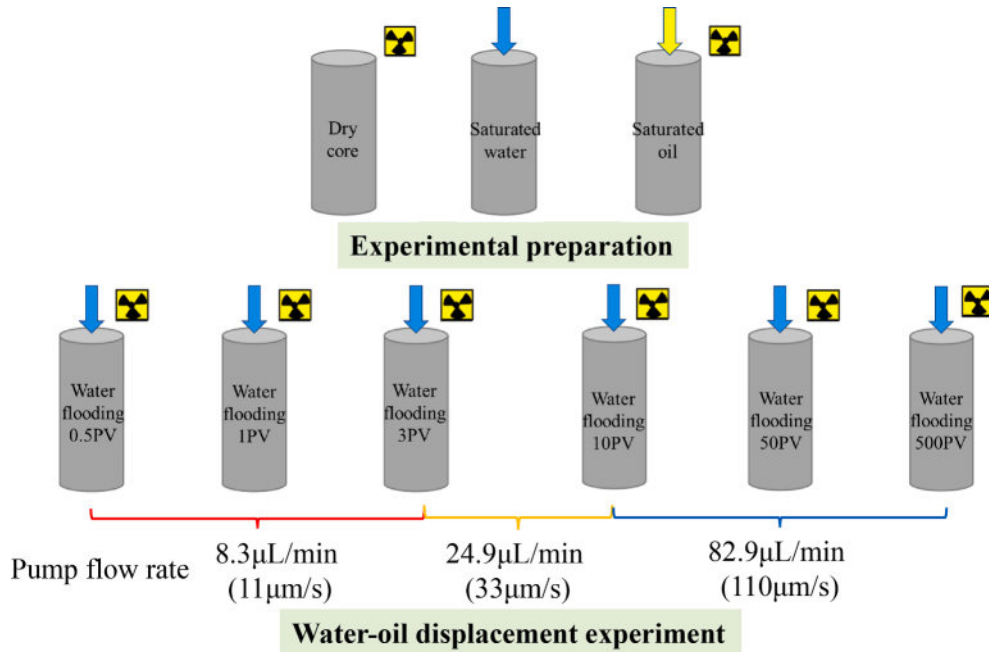


Fig. 2. Experimental process of long-term waterflooding (the Darcy velocity related to the pump flow rate is indicated in parentheses).

and 500PV. Before CT scanning, we shut off the fluid injection and discharge, and maintain the brine-oil distribution in the core sample with the confining pressure for 0.5 h, which is required to suppress the influence of fluid movement and ensure the accuracy of the image scanning. Three sequential injections with different velocities were performed during the whole waterflooding experiment, containing the first stage from 0PV to 3PV with a pump flow rate of $8.3 \mu\text{L}/\text{min}$, the second stage from 3PV to 10 PV with a pump flow rate of $24.9 \mu\text{L}/\text{min}$, and third stage from 10PV to 500PV with a pump flow rate of $82.9 \mu\text{L}/\text{min}$.

2.3. Imaging process on CT data

The 3D images reconstructed from the CT scanning test cannot be used directly, because uncontrollable factors such as X-ray source intensity, rock physical properties, and external environment will cause the narrow threshold distribution, noise, beam hardening, and ring artifacts in the images. These issues affect the precision and accuracy of subsequent image segmentation. Therefore, the CT scanning data of natural sandstone in the waterflooding experiment will be optimized first, including threshold brightness adjustment, voxel noise removal, and beam-hardening improvement. Herein, the non-local homogeneous filtering was performed on the 3D images.

The CT scanning images mainly contain information of water, oil,

and rock matrix. The rock matrix is composed of a mixture of various minerals with a wide distribution of gray values in CT images. Thus, the gray value of the water-oil interface will overlap with the rock matrix, and it is not easy to identify the boundaries between different phases. The global threshold segmentation method is unable to effectively segment the water, oil, and rock matrix in the CT images. To accurately obtain the spatial distribution of different phases in the CT images, we use the watershed algorithm in the open-source code Porespy for image segmentation. The water-oil-solid three phases are extracted from the digital rocks of sandstone cores with various permeability at seven displacement stages (i.e., 0PV, 0.5PV, 1PV, 3PV, 10PV, 50PV, and 500PV). We segmented each 3D gray image into the 3D pore structure digital rock and the residual oil digital rock, as shown in Fig. 3. These digital rocks could provide reliable basic data for subsequent analysis in the dynamic variation of residual oil, fluid displacement and trapping mechanism at the pore scale.

3. Results and discussion

3.1. Characterization of residual oil

The digital morphology of the oil phase and its variation in the sample Rock 1 during waterflooding is displayed intuitively in Fig. 4, where the isolated oil cluster are labeled with random colors. The

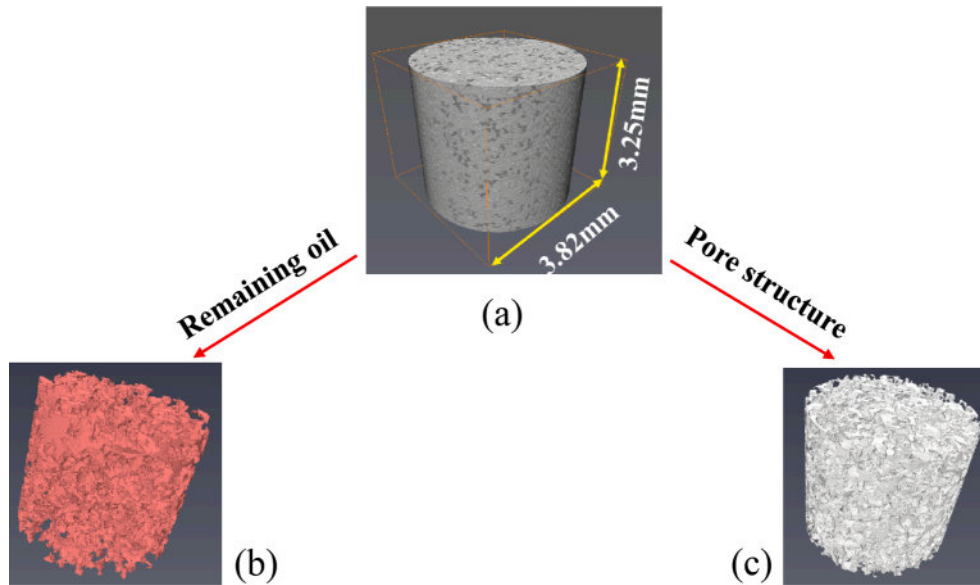


Fig. 3. Extraction of residual oil and pore structure: (a) gray distribution of digital rock, (b) residual oil distribution, (c) 3D pore structure.

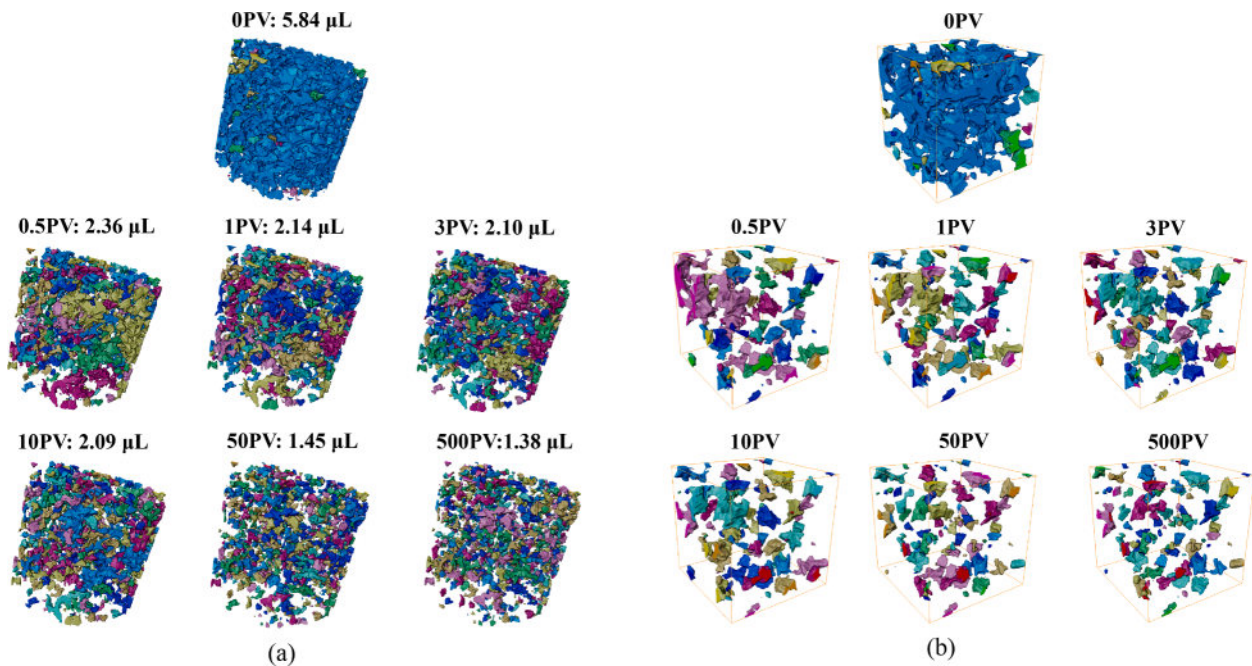


Fig. 4. Visualization of the residual oil in sandstone core Rock 1 during long-term waterflooding. The colorful parts stand for the residual oil: (a) the whole core sample; (b) the cube subset sample with a side size of 0.7 mm.

snapshots indicate there is a main oil cluster (blue color) through the porous media at 0 PV, and it is broken into numerous oil droplets from 0.5 PV to 500 PV, and the size of the largest oil cluster becomes smaller. A comparison of the oil phase in the cubic subset sample indicates that the volume oil phase decreases and the oil cluster becomes more dispersed during long-term waterflooding, as shown in Fig. 4 (b). Most of the oil resident in the core sample was displaced in the first waterflooding stage (0.5PV), and long-term waterflooding and increasing injecting velocity also enhanced the displacement efficiency of the residual oil in porous media. To quantify the dynamic variation of the oil phase trapped in the sandstone cores, the volumes of oil saturated in the three cores at the initial displacement stage are calculated and they are 5.83, 5.37, 4.16 μL , as shown in Fig. 5(a). In the Rock 1, the oil volume of 5.83 μL at the initial stage (0PV) is reduced to 2.36 μL after 0.5PV water

injection. Ultimately, 1.38 μL of oil phase remains when applying the enhanced strategies of long-term waterflooding and increasing injecting velocity. The quantitative variation of oil volume in Rock 1 demonstrates the impact of enhanced strategies used in this study. The waterflooding process from 0.5PV to 3PV has a slight effect on the residual oil recovery in the three sandstone rocks. When the injecting velocity increases to 33 $\mu\text{m/s}$, the extracted oil volume in this stage is larger in the lower-permeability core. The long-term waterflooding process also makes a slight impact on the oil volume trapped in the rock pore structure. Compared to the oil volume variation during long-term waterflooding, the number of residual oil clusters varies even more, as shown in Fig. 5(b). Based on the 3D binary images for oil phase segmented from the gray images of digital rock, the plugin MorphoLibJ in the opensource software Fiji (<https://imagej.net/imagej-wiki-stat>

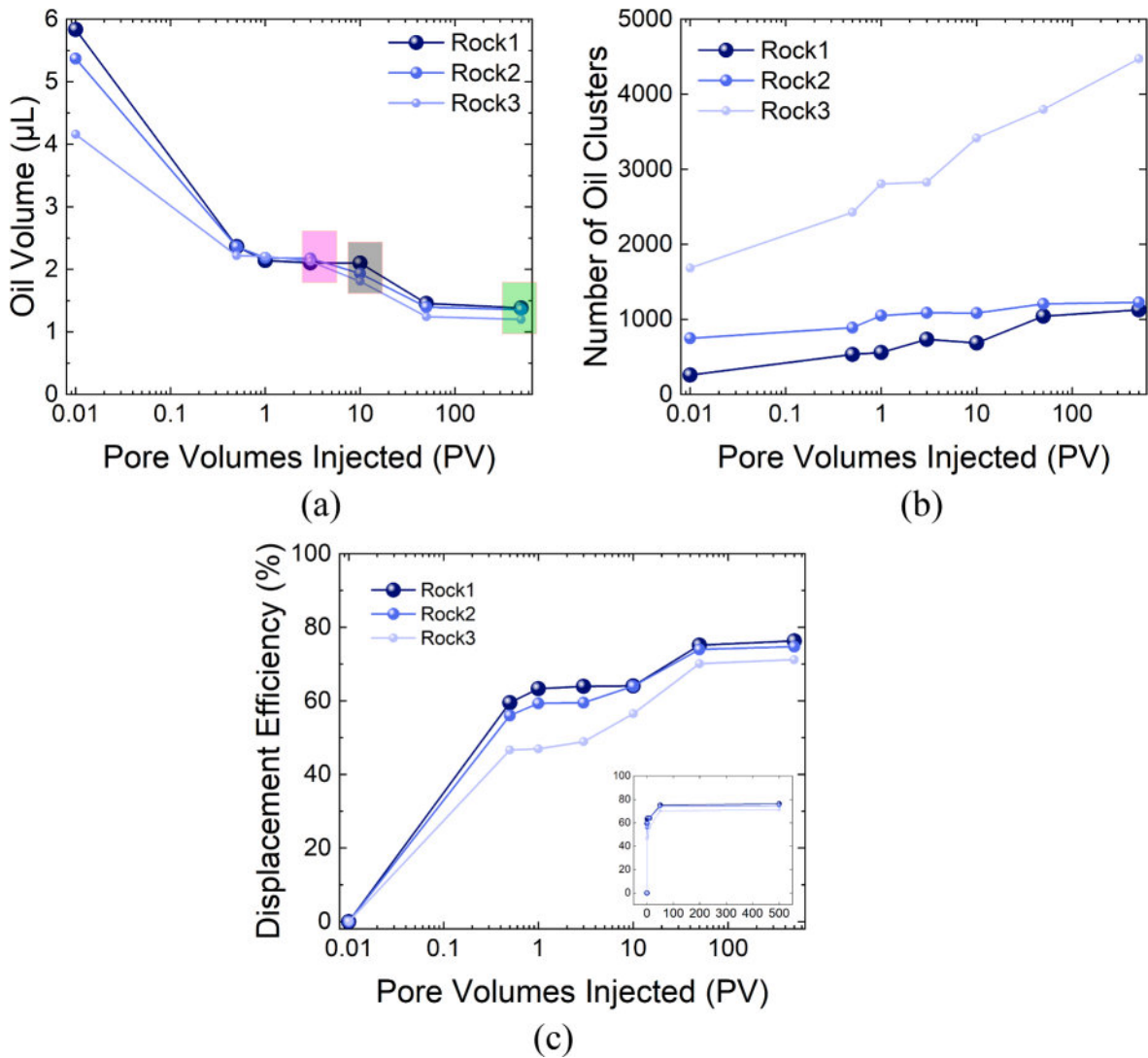


Fig. 5. The dynamic variation of residual oil during long-term waterflooding in various heterogeneous pore structures: (a) oil volume variation, (b) oil cluster number variation, and (c) oil displacement efficiency variation.

ic/Fiji) is used to identify the oil cluster by searching the connected components for each voxel. The initial oil phase breaks into more tiny droplets in the lower-permeability core, it could be ascribed to the more complex heterogeneity of pore structure in Rock 3. There is a significant change in the residual oil number from 50PV to 500PV owing to the long-term waterflooding, although the oil volume remains almost unchanged. We also depicted the displacement efficiency of the oil phase during the water–oil displacement process in Fig. 5 (c). The semi-logarithmic figure reflects that the strategies of the long-term PV injection and increasing the injecting velocity affected the residual oil mobilization, and the trapped oil varies more dramatically in the lower-permeability core during the whole displacement process. The normal-axis subfigure indicates that most of the oil phases were extracted at the initial waterflooding stages, and the efficiency of enhanced oil recovery keeps almost constant. Thus, it's vital to propose more economic and effective strategies in the exploitation of the subsurface hydrocarbon resources, which requires further understanding of the residual-oil displacement mechanism at the pore scale.

The heterogeneity of pore structure in the sandstone rock induces the complex behaviors of the water–oil interface and versatile distribution of residual oil during the waterflooding displacement. The residual oil phase in the pore structure is split into plenty of isolated oil clusters that are marked with different numbers. We made a statistical analysis in the

size and volume distribution of the oil cluster at each waterflooding stage, as shown in Fig. 6. At the initial stage (0PV), the oil phase features with large size cluster and considerable small droplets. The results indicate that the oil phase breaks up into oil clusters with smaller sizes during the waterflooding. Increasing injecting velocity provides enough waterflooding energy, leading to the volume reduction of large oil clusters and the number fraction increase of small oil clusters at 10PV and 50PV. The long-term waterflooding from 50PV to 500PV changed the number fraction distribution of the oil cluster and has an insignificant effect on the oil volume distribution. A comparison of the oil cluster size and volume distribution shows a similar displacement mechanism of the residual oil in the different sandstone cores. Especially, the dominant size of residual oil at 500PV in the Rock 3 is smaller than that in the Rock 1 with higher permeability, which could be ascribed to the constraints of the pore structure characteristics.

3.2. Characteristics of pore space occupied by residual oil

The morphology of the pore heterogeneity constrains the displacement behaviors and leads to a versatile distribution of residual oil, such as adhering to the pore wall and pore corners and retaining in pores and throats. The occurrence state of the residual oil in the subsurface reservoir is related to the characteristics of the rock pore structure. The

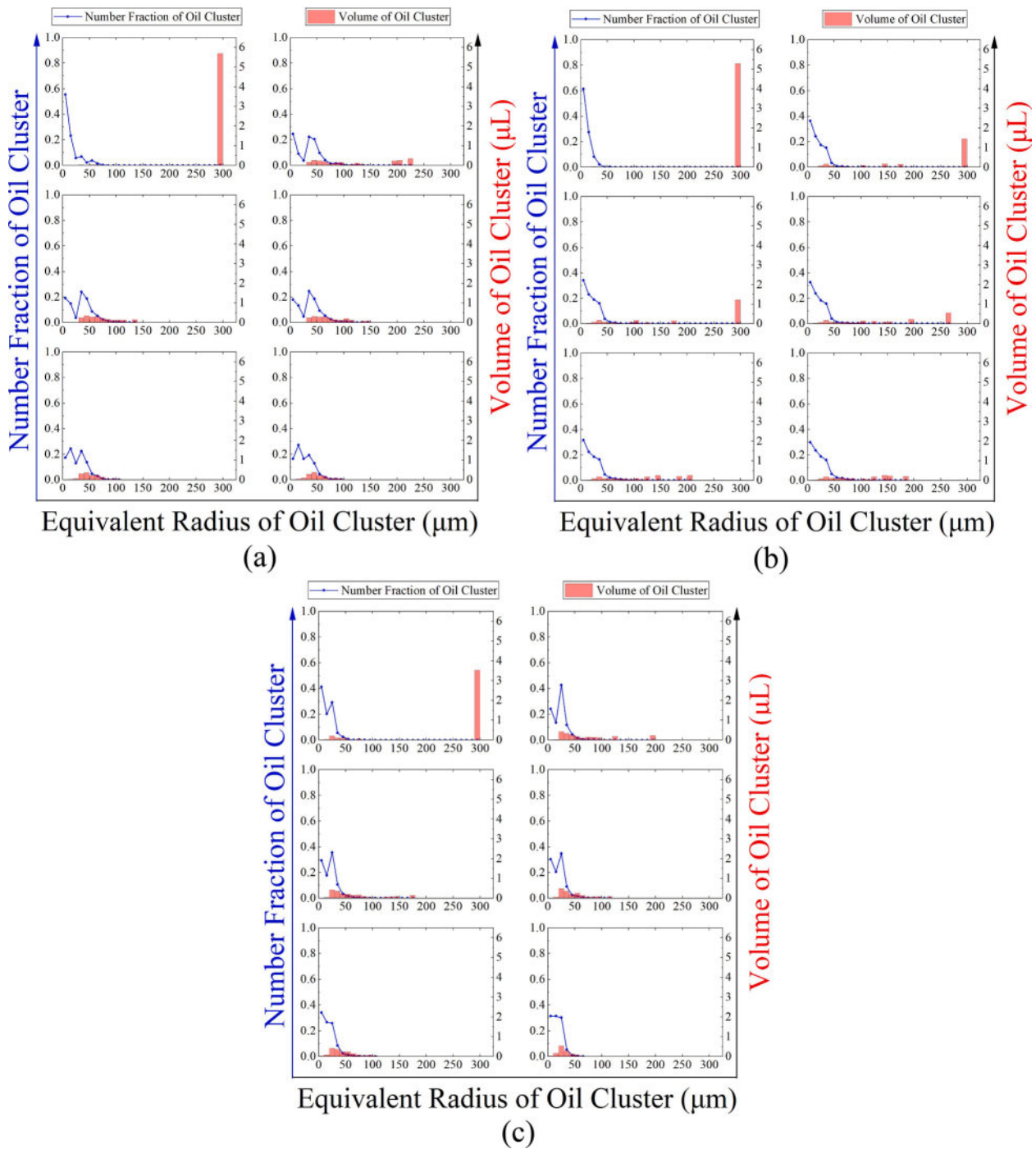


Fig. 6. The dynamic variation of number and volume distribution of residual oil during waterflooding in different pore structures: (a) Rock 1, (b) Rock 2, (c) Rock 3.

pores and throats were extracted from the digital rock of the pore structure using the open-source code LoREPorTS [47], and the size distribution of the void space residual oil phase and the volume distribution of the remained oil phase were analyzed. In Fig. 7, we quantify the dynamic variation of residual oil and the occupying void space at the initial state (OPV) and final state (500PV). The figure reflects the residual oil mobilization after performing increasing injecting velocity and long-term waterflooding in the different heterogeneous pore structures. In Fig. 7(a1)–(c1), the residual oil mobilization occurs in the pores with a wide size distribution. Owing to the constraints of the pore space in the different sandstone cores, the size distribution of pore space occupied by the oil phase is lower in the lower-permeability core. The largest sizes of pores containing oil phase are 240 μm , 160 μm , and 130 μm in Rock 1,

Rock 2, and Rock 3, respectively. Similarly, the oil phase trapped in the large pores made a major contribution to the oil volume reduction and enhanced oil recovery in each rock. Moreover, the volume distribution of oil phase retaining in the throats and the corresponding throat size distribution have the same trend as those in the pores of sandstone cores, as shown in Fig. 7(a2)–(c2).

The oil volumes displaced in the pore zones are 2.84, 2.15, and 2.04 mm^3 in sandstone cores Rock 1, Rock 2, and Rock 3, respectively. The corresponding oil volumes displaced in the throat zones are 1.62, 1.46, and 0.92 mm^3 . To quantify the displacement efficiency in the local void zones, we segmented the pore structure into a series of void groups with a certain range of void diameter and calculated the volume summary of residual oil occupying the segmented void groups (including pores and

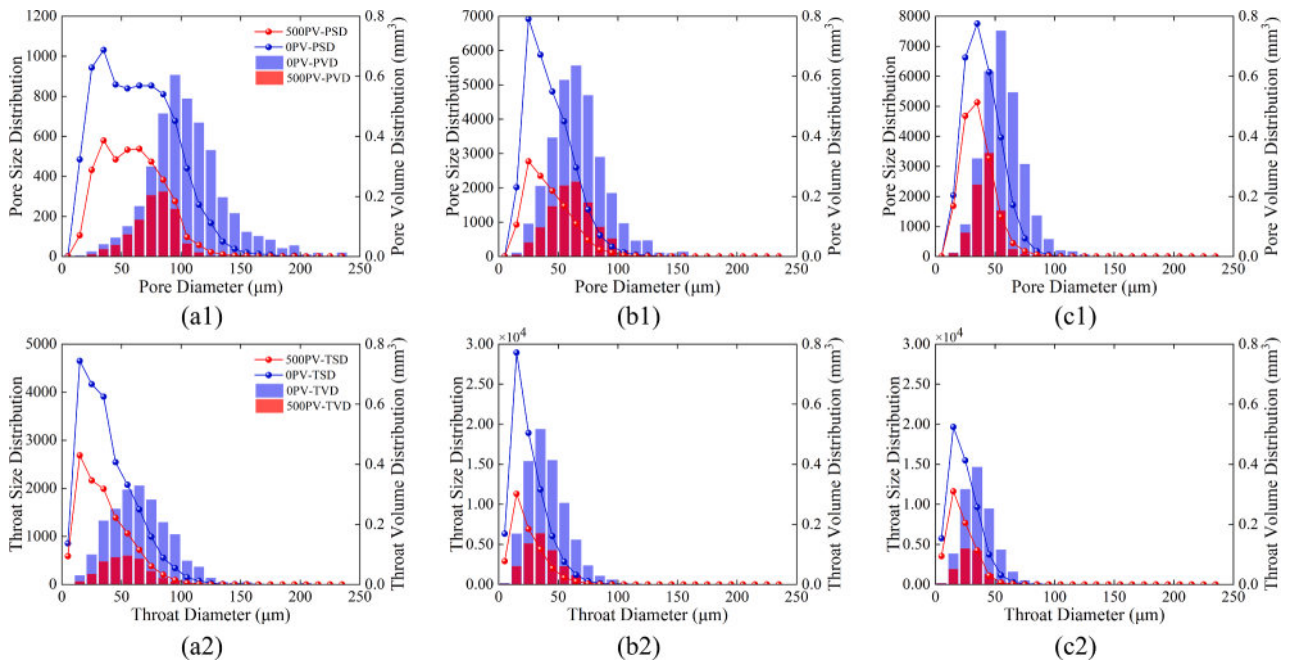


Fig. 7. Dynamic variation of pore space occupied by residual oil in heterogeneous pore structures: (a1)–(c1) for pore body, and (a2)–(c2) for pore throat in the three rock samples, respectively.

throats). We define the volume ratio of the oil phase between the initial stage and alternative waterflooding stage in the void groups as the local oil saturation. Fig. 8 shows a comparison of the distributions of local oil saturation at different waterflooding stages (3PV, 10PV, 50PV, 500PV) for different sandstone cores. A comparison of red and blue curves in Fig. 8 reflects that the increasing injecting velocity has a negligible effect on the local oil saturation in Rock 1 and shows a great impact in Rock 3. When providing enough injecting energy with a velocity of 110 $\mu\text{m/s}$ and performing long-term waterflooding, the local oil saturation in the segmented void zones reduces significantly in all the sandstone cores. Even though performing the same strategies in the waterflooding process, the pore size trapping the oil phase is larger in Rock 1 with higher permeability.

3.3. Quantitative variation of residual oil

Owing to the occurrence of a preferential flow pathway, it is challenging to recover the whole of the residual oil and improve the displacement efficiency in porous media. Thus, it is prevalent to categorize the residual oil and pay attention to the dominant oil type. The dominant residual oil could be extracted by performing the targeted displacement strategies. The previous studies mainly focused on the

understanding of morphological characteristics and storing location of the residual oil in the pore structure. The corresponding measures were proposed empirically to improve displacement efficiency and it lacks a theoretical basis. Herein, we tend to solidify the relationship between the forces acting on the residual oil and their geometrical characteristics, and then inspire the targeted displacement strategies from the perspective of the force balance exerted on the residual oil in the heterogeneous pore structures. Therefore, we proposed a new classification of the residual oil considering their occurrence state and force balance in porous media.

Fig. 9 shows the conceptual models for diverse types of residual oil (i. e., Type A, Type B, Type C, Type D, and Type E). The residual oil mobilization can be quantitatively understood by balancing the viscous forces exerted on the isolated oil phase with the pore-scale capillary forces that keep them trapped within the medium, as well as the shear force on the immiscible interface. The gravity could be ignored in this study because the Bond number ($Bo = \frac{\Delta\rho g R^2}{\sigma}$) is about 10^{-4} , where the density difference of oil and water $\Delta\rho = 280 \text{ kg/m}^3$, we choose the average pore size ($R = 50 \mu\text{m}$) as the characteristic length, and the interface surface $\sigma = 30 \text{ mN/m}$. We select three geometrical parameters to categorize the residual oil, including the number of water–oil interface, the specific surface area of oil, and the water–oil area ratio. The

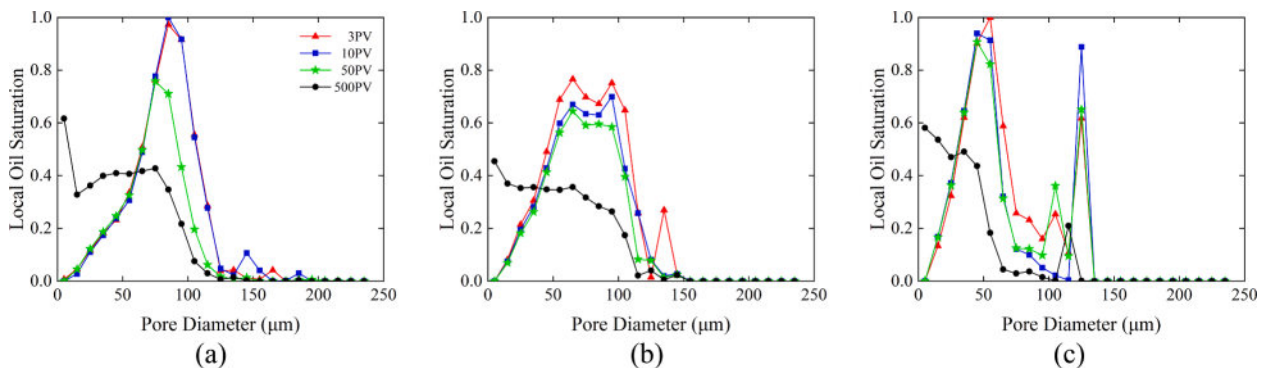


Fig. 8. The effect of long-term waterflooding and increasing injecting velocity on local saturation distribution.

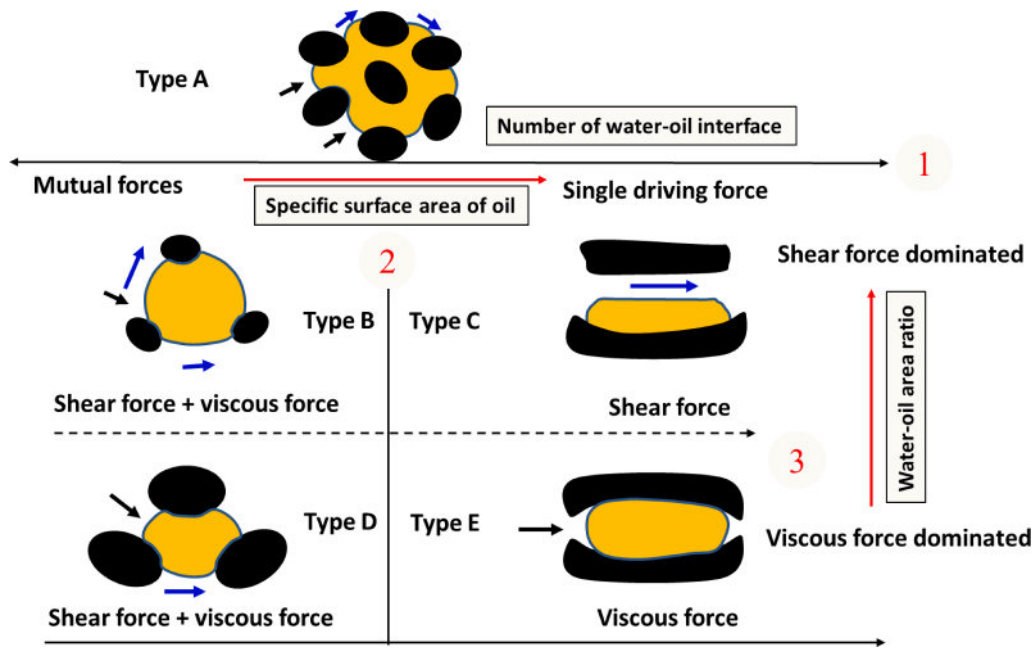


Fig. 9. The category of residual oil (Type A–Type E). The black part represents the solid and the yellow part is for the residual oil, the blue arrow stands for shear force and the black one is for viscous force.

number of water–oil interface stands for the number of water–oil displacement pathways and describes its sweeping potential in the pore structure. The residual oil with a considerable number of water–oil interface usually occupies multiple pores and the viscous force exerted on the oil cluster could push a part of the oil phase, leading to a short preferential path. In this condition, the shear force is regarded as the resistance to suppress the interface motion, this kind of residual oil is labeled as Type A. The specific surface area is the surface area per unit volume of the isolated residual oil, and it reflects the force type acting on the residual oil. The residual oil with a large specific surface area owns enough surface area, such as adhering to the pore wall or retaining in a slit pore, wherein a single driving force is determined from the forces balance during waterflooding. On the contrary, the residual oil with a small specific area is subjected to mutual driving forces including viscous and shear forces. The water–oil area ratio is calculated as the ratio of the water–oil interface area and oil surface area, and it indicates the dominant type of forces driving the residual oil. The residual oil with a large water–oil area ratio has an adequate interface to provide a shear force, which means the shear force is dominant in the forces acting on the residual oil. Otherwise, a small water–oil area ratio indicates that the pore wall occupies the most surface of the residual oil, and the shear force is weak. We categorize the residual oil into five types and summarize their geometrical characteristics and force balance, as shown in Table 2. Each residual oil has its typical force balance. The pore-scale displacement criteria are based on that the driving force is large than

the resistance. Thus, we could design different enhanced-oil-recovery strategies to unbalance the occurrence state of the residual oil and satisfy the inequal formulations.

To categorize the residual oil during the long-term waterflooding in the sandstone cores, determining the critical value is vital to identify the different oil types. The purpose of the residual oil classification is to determine the major part with similar dynamics characteristics among them and then to design the targeted displacement strategies. In doing so, we obtain an approach from econometrics and statistics, i.e., an approximate sign test for the continuity of a density (g-order statistics) [48]. The construction of this test is based on a simple intuition that, when the density of the factor (or variable) is discontinuous at the cut-off (in our case, it refers to number of water–oil interface, water–oil area ratio, or specific surface area), the fraction of left-side and right-side units to the cut-off should be statistically different. In our work, we test whether the fraction of left-side and right-side units to the cut-off were statistically different at each 0.01 step forward. Taking Rock 1 as an example, to approximate the cut-off at C1, we tested each candidate cut-off from 0, 0.01, 0.02, ..., to 99.98, 99.99, and 100. And we finally found that when number of water–oil interface equals 45, the left-side and right-side units to the cut-off were statistically different (p-value < 0.01). Hence, the critical value in terms of the number of water–oil interface is determined statistically to distinguish the major part and minor part of the residual oil. The mathematical details and steps can be found in the p.142 in Bugnia and Canay’s paper [48]. In practice, this

Table 2
The category of residual oil and its mobilization condition.

Residual oil category		Mobilization condition			
Oil Type	Categorizing parameters and micro-forces				Driving force > resistance
Type A	Large number of water–oil interface				$P_v > P_s + P_c$
Type B	Small number of water–oil interface	Small specific surface area	Mutual forces	Large water–oil area ratio	Shear force dominated
Type C		Large specific surface area	Single force	Large water–oil area ratio	Shear force dominated
Type D		Small specific surface area	Mutual forces	Small water–oil area ratio	Viscous force dominated
Type E		Large specific surface area	Single force	Small water–oil area ratio	Viscous force dominated
					$P_v + P_s > P_c$
					$P_v > P_c$

test can be processed using package “RDCONT” via STATA v.16 or above [49].

Similarly, we could find the critical values for three quantitative parameters based on the geometrical data of residual oil at the final stage in different sandstone cores, as shown in Fig. 10, and the corresponding results are summarized in Table 3. In the sandstone core with lower permeability, the critical value C_1 for the number of water–oil interface increases, C_2 for the water–oil area ratio decreases, and C_3 for specific surface area increases.

Fig. 11 shows the dynamic variation of diverse types of residual oil in the different sandstone cores from the perspective of the number percentage and volume of residual oil. We could observe that five types of residual oil all exist in the sandstone cores. The number percentage of residual oil varies slightly from OPV to 500PV for the diverse types of oil, and the volume of different types of oil changes significantly. The dominant-oil type is determined as the oil type with the largest oil volume at the final stage of waterflooding. Thus, we find that the dominant types are Type D, Type A, and Type E in Rock 1, Rock 2, and Rock 3, respectively. As abovementioned, the geometrical characteristics of Type D of residual oil feature a small water–oil area ratio and small specific surface area, and its force balance is comprised of the viscous-driving force and capillary resistance. Hence, it is reasonable to enhance the viscous force or decrease the capillary force to satisfy the mobilization condition of Type D in Table 2. Similarly, we give the dominant oil type, geometrical characteristics, force balance, and the corresponding mobilization strategies for the residual oil in Rock 2 and Rock 3, as shown in Table 4.

3.4. Validation of the residual oil mobilization

Because of the alleviative expense on computational resources of direct numerical simulation in a large computational domain, the pore network model becomes an effective approach to simulate the multiphase flow in porous media [50–53]. The pore network model contains two parts: pore network extraction and pore network modeling. The heterogeneous pore structure is simplified into the pore network, and it is composed of a series of pores and throats with a certain volume and flow resistance. Herein, we used the open-source code LoREPorTS to extract the pore network based on local hydraulic resistance equivalence between the real space and the pore-throat geometry, and the details are introduced in Liu et al.’s work [47]. The pore network segmented from the 3D images of sandstone cores is displayed in Fig. 12. It shows that the pore network in the core with higher permeability owns fewer pores and large size. Unlike the quasi-static pore-network model to simulate the equilibrium states which is controlled by entry capillary pressure only, here we apply the dynamic pore-network model to consider the competition between viscous forces, shear forces, and capillary forces on residual oil mobilization. The fundamentals of the dynamic pore-network model are introduced in the works [54,55].

To validate the mobilization strategies of the residual oil in different

Table 3

The critical value of quantitative parameters in different sandstone rock samples.

Rock samples	Number of water–oil interface C_1	Water–oil area ratio C_2	Specific surface area C_3
Rock 1	23	0.24	0.41
Rock 2	40	0.15	0.47
Rock 3	45	0.14	0.5

sandstone cores, we performed the dynamic pore network modeling on the three cores with different permeability. Particularly, the spatial distributions of water, oil, and pore structure at 500PV of the waterflooding experiment are input as the initial condition in the pore-scale simulations. To unbalance the force state of the residual oil at the final stage of waterflooding experiment in the simulations, we increased the injecting velocity to 220 $\mu\text{m/s}$ in Rock 1 for increased viscous force, decreased the water-wet contact angle to 23° (the strong water-wet condition) in Rock 2 for a positive capillary force, and decreased interface tension to 1mN/m in Rock 3 for decreased capillary force. We set the fixed velocity boundary condition at the inlet and the zero pressure-gradient boundary condition at the outlet of the pore structure in the sandstone cores. The dynamic pore network modeling ends when the tolerance of oil saturation in the whole pore structure is smaller than 10^{-7} . Fig. 13 displays the spatial distribution of the oil phase trapped in different cores after numerically performing mobilization strategies. The volume of the oil phase trapped in porous media is 1.38, 1.75, and 1.19 μL at 500PV in Rock 1, Rock 2, and Rock 3, respectively. The corresponding oil volume in simulations is 0.17, 0.26, and 0.52 μL . Therefore, the enhanced oil recovery is 21 %, 28 %, and 17 % in Rock 1, Rock 2, and Rock 3, respectively.

4. Conclusions

This study performed long-term water–oil displacement experiments in the three natural sandstone cores with different heterogeneous pore structures, and quantitatively analyzed the dynamic variation of the distribution and saturation of the residual oil. During the waterflooding process, the volume and cluster number of the trapped oil varies more dramatically in the lower-permeability core. The strategy of increasing injecting velocity has a more muted effect on the local oil saturation in the higher-permeability core. The strategy of long-term waterflooding changes the number fraction distribution of the oil cluster and has a significant effect on the local oil saturation in the divided pore zones.

To quantify the dynamic variation of the residual oil at the pore scale, this study presents a novel classification of oil clusters trapped in the heterogeneous pore structure by establishing the relationship between morphological characteristics and force balance including viscous force, shear force, and capillary force. The residual oil is classified into five types, and the significant difference in statistical evaluation is

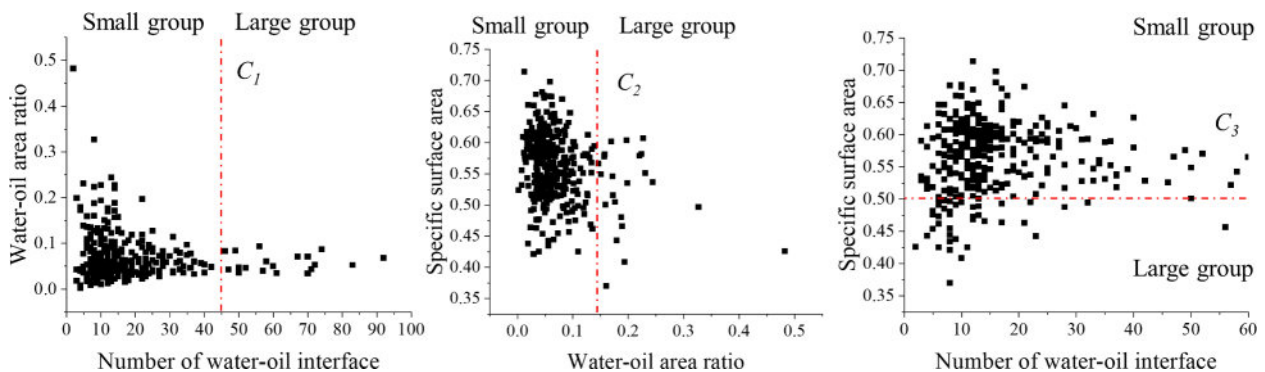


Fig. 10. Determination of critical value for quantitative parameters in the classification of the residual oil.

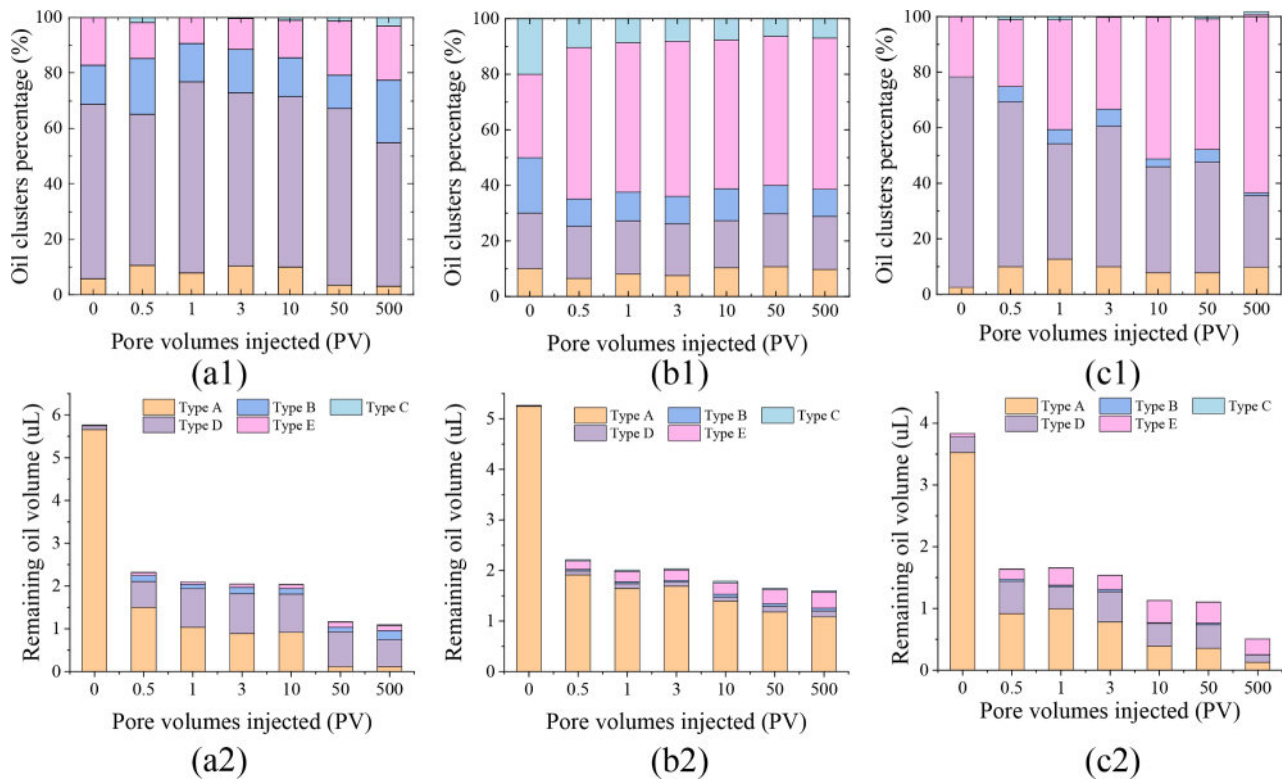


Fig. 11. The dynamic variation of different types of residual oil in the sandstone cores: (a1)–(c1) represent the volume variation, and (a2)–(c2) are for the number percentage variation of residual oil during long-term waterflooding.

Table 4
The dominant residual oil and the corresponding mobilization strategies in different rock samples.

Rock sample	Rock 1	Rock 2	Rock 3
Permeability (mD)	7449	1594	908
Dominant oil type	Type D	Type A	Type E
Geometrical characteristics	Small water–oil area ratio Small specific surface area	Large number of water–oil interface	Small water–oil area ratio Large specific surface area
Micro-force balance	Viscous force driving Capillary resistance	Viscous force driving Shear and capillary resistance	Viscous force driving capillary resistance
Mobilization strategy	Decrease capillary force. Increase viscous force	Decrease shear and capillary force. Increase viscous force	Decrease capillary force. Increase viscous force

applied to determine the critical value for different types of residual oil. The quantitative analysis in the different types of residual oil demonstrated that the sandstone cores with different permeability feature various oil types dominated in the residual oil clusters after the long-term waterflooding, which is affected by the pore structure heterogeneity. The experimental and numerical results in the multiphase displacement process showed it was challenging to extract all the oil clusters trapped in the heterogeneous pore structure and the dominant type of residual oil with large oil volume should become the primary object for the oil mobilization. The results from the dynamic pore network modeling of water–oil displacement proved that the dominant part with similar kinetic characteristics among the residual oil in porous media could be recovered and a higher oil recovery was achieved using the targeted strategies of oil mobilization from the perspective of force balance at the pore scale.

The classification of the residual oil in porous media proposed in this

study helps us understand the dynamic state of dominant part in the residual oil and has a strong capability to assist in the strategy design of enhanced oil recovery. From the perspective of force balance at pore scale, the inertial force and gravity are neglected concerning the low capillary number and low Bond number. We also recognize that the characteristics of the dominant residual oil are affected by the permeability and heterogeneity of pore structure, injection conditions, and fluid properties. At present, the change and factors of residual oil type have not been understood at pore scale, leading to challenges to predict directly the dominant characteristics of residual oil in porous media. In the future, based on quantitative characterization approach proposed, the type of oil clusters could be identified during immiscible displacement in porous media, and it is convenient to record the dynamic behaviors of the trapped oil cluster in heterogeneous pore structure using the experimental and numerical methods. Hence, the key factor in the dominant characteristics of trapped fluid and its remobilization mechanism will be revealed at pore scale.

CRedit authorship contribution statement

Wenbo Gong: Writing – original draft, Methodology, Investigation. **Yang Liu:** Methodology. **Chaodong Xi:** Data curation. **Guang Yang:** Software. **Yang Ju:** Methodology. **Moran Wang:** Writing – review & editing, Writing – original draft, Supervision, Project administration, Conceptualization.

Declaration of Competing Interest

The authors declare that they have no known competing financial interests or personal relationships that could have appeared to influence the work reported in this paper.

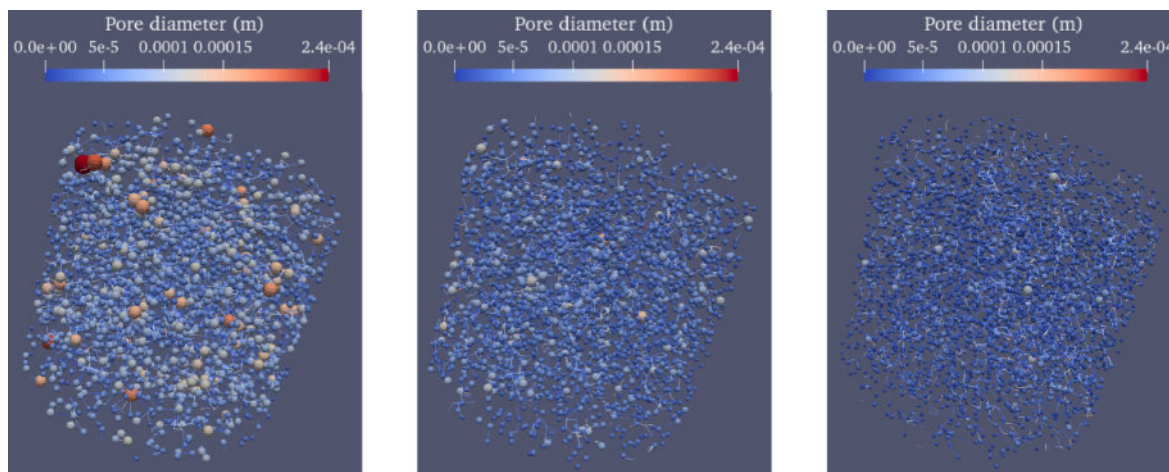


Fig. 12. Pore network extraction from sandstone cores with various permeability: (a) Rock 1, (b) Rock 2, (c) Rock 3.

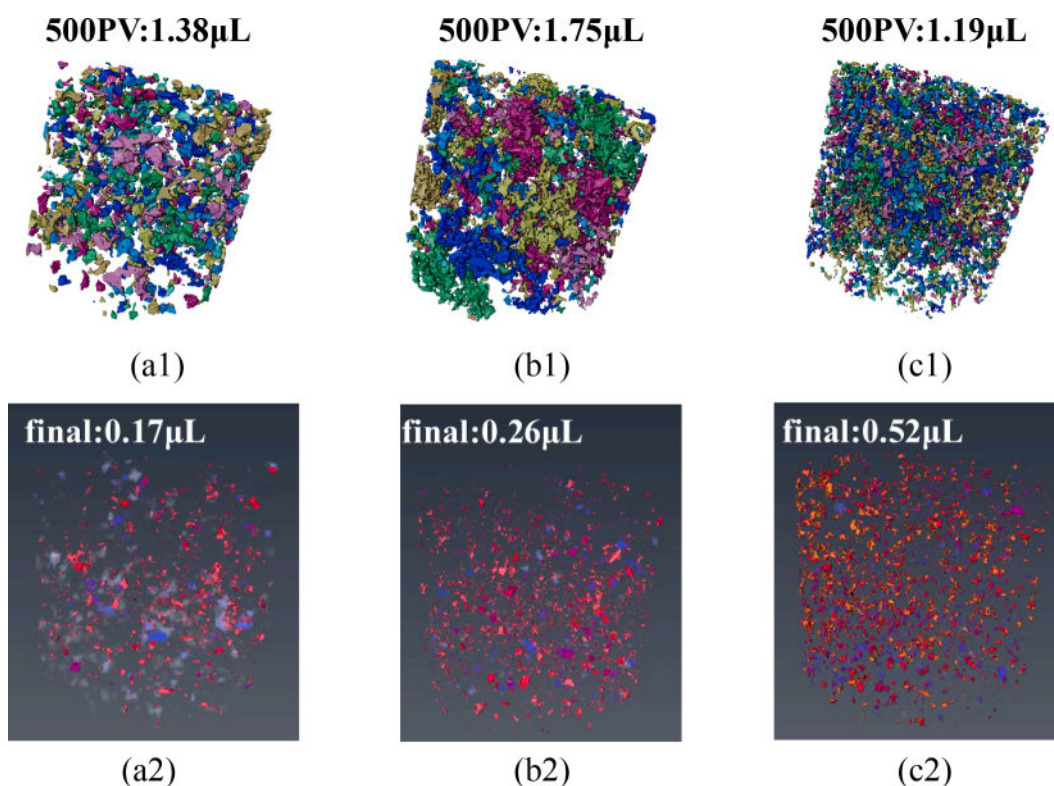


Fig. 13. The mobilization of the dominant residual oil in the different sandstone samples using the dynamic pore network model (variant colors in a2, b2, and c2 stand for the oil saturation in local pores).

Data availability

No data was used for the research described in the article.

Acknowledgments

This work is financially supported by the National Key Research and Development Program of China (No. 2019YFA0708704), the NSF grant of China (No. 12272207), and Daqing Oilfield of PetroChina.

References

- [1] Zhang N, Wang Q, Wang J, Hou L, Li H, Li Q. Characteristics of oil and gas discoveries in recent 20 years and future exploration in the world. *Pet Explor Dev* 2018;23(01):44–53.
- [2] Alfarge D, Wei M, Bai B. Chapter 6 - Water injection in unconventional reservoirs. In: Alfarge D, Wei M, Bai B, Bai B, Chen Z, editors. *Developments in petroleum science*. Elsevier; 2020. p. 113–40.
- [3] Bai Y, Hou J, Liu Y, Zhao D, Bing S, Xiao W, et al. Energy-consumption calculation and optimization method of integrated system of injection-reservoir-production in high water-cut reservoir. *Energy* 2022;239:121961.
- [4] Georgiadis A, Berg S, Makurat A, Maitland G, Ott H. Pore-scale micro-computed-tomography imaging: nonwetting-phase cluster-size distribution during drainage and imbibition. *Phys Rev E* 2013;88(3):033002.
- [5] Lei W, Liu T, Xie C, Yang H, Wu T, Wang M. Enhanced oil recovery mechanism and recovery performance of micro-gel particle suspensions by microfluidic experiments. *Energy Sci Eng* 2020;8(4):986–98.

- [6] Lei W, Lu X, Liu F, Wang M. Non-monotonic wettability effects on displacement in heterogeneous porous media. *J Fluid Mech* 2022;942:R5.
- [7] Rücker M, Bartels WB, Singh K, Brussee N, Coorn A, van der Linde HA, et al. The effect of mixed wettability on pore-scale flow regimes based on a flooding experiment in ketton limestone. *Geophys Res Lett* 2019;46(6):3225–34.
- [8] Zhao Y, Xue S, Han S, Chen Z, Liu S, Elsworth D, et al. Effects of microstructure on water imbibition in sandstones using X-ray computed tomography and neutron radiography. *J Geophys Res Solid Earth* 2017;122(7):4963–81.
- [9] Xie C, Lei W, Balhoff MT, Wang M, Chen S. Self-adaptive preferential flow control using displacing fluid with dispersed polymers in heterogeneous porous media. *J Fluid Mech* 2021;906:A10.
- [10] Xie C, Qi P, Xu K, Xu J, Balhoff MT. Oscillatory trapping of a droplet in a converging channel induced by elastic instability. *Phys Rev Lett* 2022;128(5):054502.
- [11] Han D. Discussions on concept, countermeasures and technical routes for the redevelopment of high water-cut oilfields. *Pet Explor Dev* 2010;37(05):583–91.
- [12] Mohamed AIA, Khishvand M, Piri M. The role of injection fluid elasticity in microscopic displacement efficiency of residual non-wetting phase: an in-situ experimental investigation. *Fuel* 2023;333:126180.
- [13] Lei W, Lu X, Wang M. Multiphase displacement manipulated by micro/nanoparticle suspensions in porous media via microfluidic experiments: from interface science to multiphase flow patterns. *Adv Colloid Interface Sci* 2023;311:102826.
- [14] Stone HA, Stroock AD, Ajdari A. Engineering flows in small devices: microfluidics toward a lab-on-a-chip. *Annu Rev Fluid Mech* 2004;36(1):381–411.
- [15] Blunt MJ, Bijeljic B, Dong H, Gharbi O, Iglauer S, Mostaghimi P, et al. Pore-scale imaging and modelling. *Adv Water Resour* 2013;51:197–216.
- [16] Ju Y, Gong W, Zheng J. Characterization of immiscible phase displacement in heterogeneous pore structures: parallel multicomponent lattice Boltzmann simulation and experimental validation using three-dimensional printing technology. *Int J Multiph Flow* 2019;114:50–65.
- [17] Lei W, Lu X, Wu T, Yang H, Wang M. High-performance displacement by microgel-in-oil suspension in heterogeneous porous media: Microscale visualization and quantification. *J Colloid Interface Sci* 2022;627:848–61.
- [18] Ling B, Sodwatana M, Kohli A, Ross CM, Jew A, Kovscek AR, et al. Probing multiscale dissolution dynamics in natural rocks through microfluidics and compositional analysis. *Proc Nat Acad Sci* 2022;119(32):e2122520119.
- [19] Withjack EM. Computed tomography for rock-property determination and fluid-flow visualization. *SPE Form Eval* 1988;3(04):696–704.
- [20] Alhosani A, Bijeljic B, Blunt MJ. Pore-scale imaging and analysis of wettability order, trapping and displacement in three-phase flow in porous media with various wettabilities. *Trans Porous Media* 2021;140(1):59–84.
- [21] Ju Y, Xi C, Zheng J, Gong W, Wu J, Wang S, et al. Study on three-dimensional immiscible water–oil two-phase displacement and trapping in deformed pore structures subjected to varying geostress via in situ computed tomography scanning and additively printed models. *Int J Eng Sci* 2022;171:103615.
- [22] Spurin C, Bultreys T, Rücker M, Garfi G, Schlepütz CM, Novak V, et al. Real-time imaging reveals distinct pore-scale dynamics during transient and equilibrium subsurface multiphase flow. *Water Resour Res* 2020;56(12):e2020WR028287.
- [23] Berg S, Ott H, Klapp SA, Schwing A, Neiteler R, Brussee N, et al. Real-time 3D imaging of Haines jumps in porous media flow. *Proc Nat Acad Sci* 2013;110(10):3755–9.
- [24] Al-Bayati D, Saedi A, Myers M, White C, Xie Q. An experimental investigation of immiscible CO₂ flooding efficiency in sandstone reservoirs: influence of permeability heterogeneity. In: *SPE Europe featured at 80th EAGE conference and exhibition*; 2018. p. D041S09R07.
- [25] Arshadi M, Gesho M, Qin T, Goual L, Piri M. Impact of mineralogy and wettability on pore-scale displacement of NAPLs in heterogeneous porous media. *J Contam Hydrol* 2020;230:103599.
- [26] Liu F, Wang M. Wettability effects on mobilization of ganglia during displacement. *Int J Mech Sci* 2022;215:106933.
- [27] Mazinani S, Farhadi H, Fatemi M. Experimental and theoretical investigation of the impact of crude-oil on the wettability behavior of calcite and silicate due to low salinity effect. *Fuel* 2023;349:128608.
- [28] Hou J, Qiu M, Lu N, Qu Y, Li F, Meng X, et al. Characterization of residual oil microdistribution at pore scale using computerized tomography. *Acta Pet Sin* 2014;35(02):319–25.
- [29] Li J, Jiang H, Wang C, Zhao Y, Gao Y, Pei Y, et al. Pore-scale investigation of microscopic remaining oil variation characteristics in water-wet sandstone using CT scanning. *J Nat Gas Sci Eng* 2017;48:36–45.
- [30] Zhao Y, Jiang H, Li J, Wang C, Gao Y, Yu F, et al. Study on the classification and formation mechanism of microscopic remaining oil in high water cut stage based on machine learning. In: *Abu Dhabi international petroleum exhibition & conference*; 2017. p. D031S77R02.
- [31] Fang Y, Yang E, Guo S, Cui C, Zhou C. Study on micro remaining oil distribution of polymer flooding in Class-II B oil layer of Daqing Oilfield. *Energy* 2022;254:124479.
- [32] Guo C, Wang X, Wang H, He S, Liu H, Zhu P. Effect of pore structure on displacement efficiency and oil-cluster morphology by using micro computed tomography (μ CT) technique. *Fuel* 2018;230:430–9.
- [33] Li J, Liu Y, Gao Y, Cheng B, Meng F, Xu H. Effects of microscopic pore structure heterogeneity on the distribution and morphology of remaining oil. *Pet Explor Dev* 2018;45(6):1112–22.
- [34] Su Y, Zha M, Jiang L, Ding X, Qu J, Jin J, et al. Pore structure and fluid distribution of tight sandstone by the combined use of SEM, MICP and X-ray micro-CT. *J Pet Sci Eng* 2022;208:109241.
- [35] Wang F, Liu T, Lei W, Zhao Y, Li B, Yang G, et al. Dynamic analysis of deformation and start-up process of residual-oil droplet on wall under shear flow. *J Pet Sci Eng* 2021;199:108335.
- [36] Yang Y, Xiao W, Bernabe Y, Xie Q, Wang J, He Y, et al. Effect of pore structure and injection pressure on waterflooding in tight oil sandstone cores using NMR technique and pore network simulation. *J Pet Sci Eng* 2022;217:110886.
- [37] Datta SS, Dupin J-B, Weitz DA. Fluid breakup during simultaneous two-phase flow through a three-dimensional porous medium. *Phys Fluids* 2014;26(6):062004.
- [38] Datta SS, Ramakrishnan TS, Weitz DA. Mobilization of a trapped non-wetting fluid from a three-dimensional porous medium. *Phys Fluids* 2014;26(2):022002.
- [39] Schneider J, Priestley RD, Datta SS. Using colloidal deposition to mobilize immiscible fluids from porous media. *Phys Rev Fluids* 2021;6(1):014001.
- [40] Gao Y, Raeini AQ, Blunt MJ, Bijeljic B. Dynamic fluid configurations in steady-state two-phase flow in Bentheimer sandstone. *Phys Rev E* 2021;103(1):013110.
- [41] Lenormand R, Touboul E, Zarcone C. Numerical models and experiments on immiscible displacements in porous media. *J Fluid Mech* 1988;189:165–87.
- [42] Primkulov BK, Pahlavan AA, Fu X, Zhao B, MacMinn CW, Juanes R. Wettability and Lenormand's diagram. *J Fluid Mech* 2021;923:A34.
- [43] Zhang Y, Bijeljic B, Gao Y, Lin Q, Blunt MJ. Quantification of nonlinear multiphase flow in porous media. *Geophys Res Lett* 2021;48(5):e2020GL090477.
- [44] Ju Y, Gong W, Chang C, Xie H, Xie L, Liu P. Three-dimensional characterisation of multi-scale structures of the Silurian Longmaxi shale using focused ion beam-scanning electron microscopy and reconstruction technology. *J Nat Gas Sci Eng* 2017;46:26–37.
- [45] Qin X, Xia Y, Wu J, Sun C, Zeng J, Xu K, et al. Influence of pore morphology on permeability through digital rock modeling: new insights from the euler number and shape factor. *Energy Fuel* 2022;36(14):7519–30.
- [46] AlRatrouf A, Raeini AQ, Bijeljic B, Blunt MJ. Automatic measurement of contact angle in pore-space images. *Adv Water Resour* 2017;109:158–69.
- [47] Liu Y, Gong W, Zhao Y, Jin X, Wang M. A Pore-throat segmentation method based on local hydraulic resistance equivalence for pore-network modeling. *Water Resour Res* 2022;58(12):e2022WR033142.
- [48] Bugni FA, Canay IA. Testing continuity of a density via g-order statistics in the regression discontinuity design. *J Econ* 2021;221(1):138–59.
- [49] Canay IA, Kamat Y. Approximate permutation tests and induced order statistics in the regression discontinuity design. *Rev Econ Stud* 2017;85(3):1577–608.
- [50] Blunt MJ. Flow in porous media — pore-network models and multiphase flow. *Curr Opin Colloid Interface Sci* 2001;6(3):197–207.
- [51] Fatt I. The network model of porous media. *Trans AIME* 1956;207(01):144–81.
- [52] Joekar-Niasar V, Hassanizadeh SM, Dahle HK. Non-equilibrium effects in capillarity and interfacial area in two-phase flow: dynamic pore-network modelling. *J Fluid Mech* 2010;655:38–71.
- [53] Patzek TW. Verification of a complete pore network simulator of drainage and imbibition. *SPE J* 2001;6(02):144–56.
- [54] Chen S, Qin C, Guo B. Fully implicit dynamic pore-network modeling of two-phase flow and phase change in porous media. *Water Resour Res* 2020;56(11):e2020WR028510.
- [55] Qin C-Z, van Brummelen H. A dynamic pore-network model for spontaneous imbibition in porous media. *Adv Water Resour* 2019;133:103420.